

# Towards a Mechanistic Model of Solid-Electrolyte Interphase Formation and Evolution in Lithium-ion Batteries

Evan Walter Clark Spotte-Smith,<sup>†,‡,¶,#</sup> Ronald L. Kam,<sup>†,¶,#</sup> Daniel Barter,<sup>§</sup>  
Xiaowei Xie,<sup>†,||</sup> Tingzheng Hou,<sup>†,‡</sup> Shyam Dwaraknath,<sup>†</sup> Samuel M. Blau,<sup>§</sup> and  
Kristin A. Persson<sup>\*,‡,⊥</sup>

<sup>†</sup>*Materials Science Division, Lawrence Berkeley National Laboratory*

<sup>‡</sup>*Department of Materials Science and Engineering, University of California, Berkeley*

<sup>¶</sup>*Department of Chemical and Biomolecular Engineering, University of California, Berkeley*

<sup>§</sup>*Energy Storage and Distributed Resources, Lawrence Berkeley National Laboratory*

<sup>||</sup>*Department of Chemistry, University of California, Berkeley*

<sup>⊥</sup>*Molecular Foundry, Lawrence Berkeley National Laboratory*

# *These authors contributed equally to this work*

E-mail: kapersson@lbl.gov

## Abstract

The formation of passivation films by interfacial reactions, though critical for applications ranging from advanced alloys to electrochemical energy storage, is often poorly understood. In this work, we explore the formation of an exemplar passivation film, the solid electrolyte interphase (SEI), which is responsible for stabilizing lithium-ion batteries. Using stochastic simulations based on quantum chemical calculations and data-driven chemical reaction networks, we directly model competition between SEI

products at a mechanistic level for the first time. Our results recover the Peled-like separation of the SEI into inorganic and organic domains resulting from rich reactive competition without fitting parameters to experimental inputs. By conducting accelerated simulations at elevated temperature, we track SEI evolution, confirming the postulated reduction of lithium ethylene monocarbonate to dilithium ethylene monocarbonate and H<sub>2</sub>. These findings furnish fundamental insights into the dynamics of SEI formation and illustrate a path forward towards a predictive understanding of electrochemical passivation.

The stabilization of reactive surfaces by passivation films is a cornerstone process with myriad technological applications ranging from alloys<sup>1–3</sup> and microelectronics<sup>4–6</sup> to photovoltaics<sup>7,8</sup> and batteries.<sup>9,10</sup> While extensive efforts have been made to develop carefully controlled artificial passivation layers,<sup>11–15</sup> many technologically relevant passivation processes occur spontaneously by mechanisms that are highly sensitive to the environment.<sup>16–19</sup> Despite broad importance across chemical domains as well as decades of study, attempts to elucidate the formation mechanisms of passivity have yielded limited understanding of film growth, composition, and related functionality.<sup>20,21</sup>

The success of lithium-ion batteries (LIBs) illustrates the importance of functional surface film formation. LIB negative electrodes are critically stabilized by a nanoscale passivation layer known as the solid-electrolyte interphase (SEI), which deposits spontaneously as a result of electrolyte reduction and decomposition during initial charging cycles.<sup>9</sup> When appropriately formed, the SEI allows selective metal ion migration while preventing further electrolyte degradation,<sup>22</sup> leading to batteries with high Coulombic efficiency and long lifespans. On the other hand, when no passivating SEI forms, the reduction process continues, leading to rapid consumption of the electrolyte.<sup>20</sup> It is imperative to develop a mechanistic, predictive understanding of SEI formation - including the products that form and their contribution to the evolution and dynamics of the SEI under various operating conditions - both to gain fundamental insight into passivation processes and to enable the rational design

of energy storage technologies.

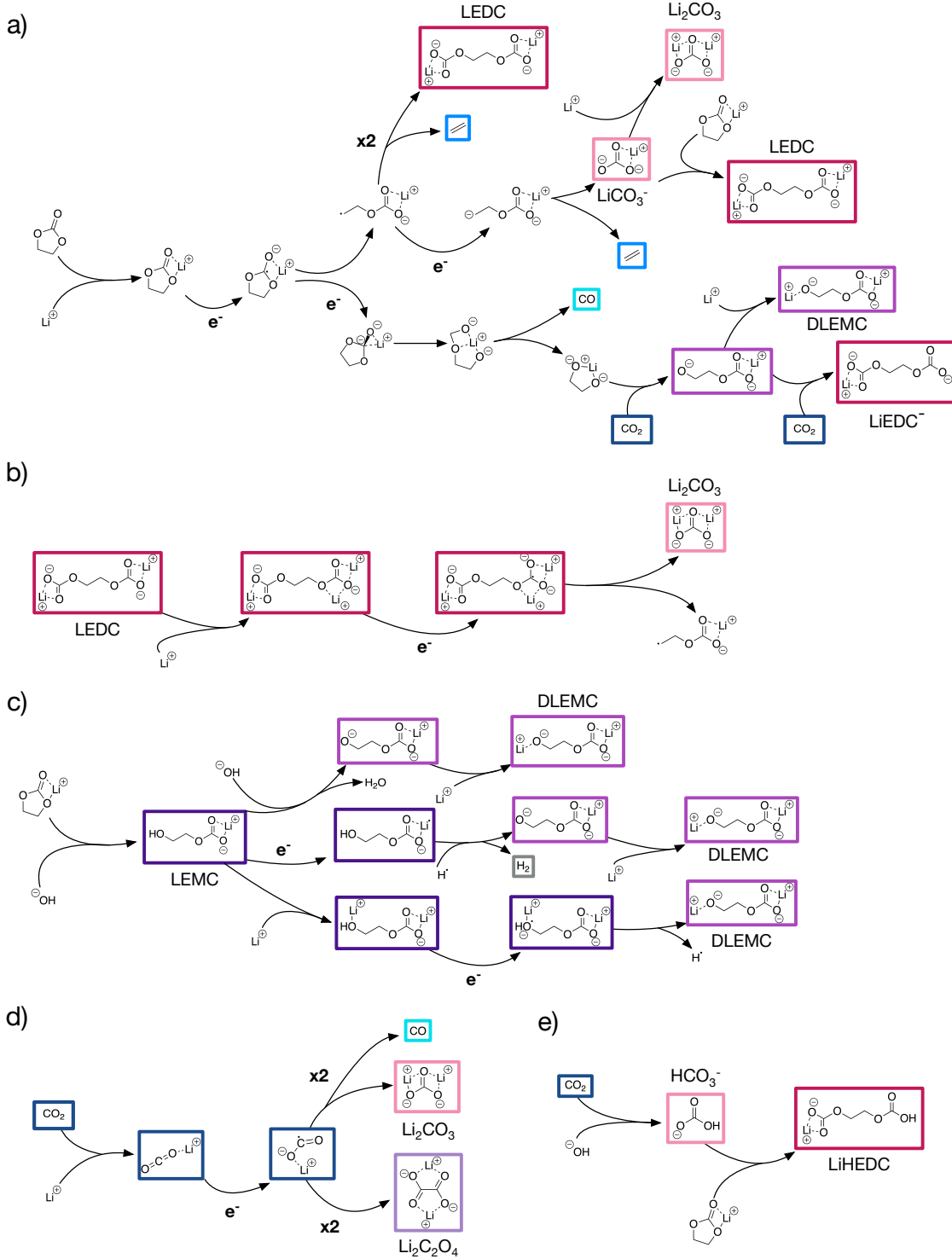
SEI layers in LIBs with ethylene carbonate (EC)-based electrolytes are made up of inorganic species - including inorganic carbonates (*e.g.* lithium carbonate ( $\text{Li}_2\text{CO}_3$ )) and lithium oxalate ( $\text{Li}_2\text{C}_2\text{O}_4$ ) - as well as organic species like *e.g.* lithium ethylene dicarbonate (LEDC) and lithium ethylene monocarbonate (LEMC).<sup>23–28</sup> The Peled model<sup>29</sup> first proposed that the SEI, though highly inhomogeneous, is comprised of a primarily inorganic inner layer and a primarily organic outer layer. It has also been observed that gases (particularly  $\text{H}_2$ ,  $\text{C}_2\text{H}_4$ ,  $\text{CO}$ , and  $\text{CO}_2$ ) are produced as byproducts of SEI formation.<sup>30,31</sup> However, in spite of decades of careful study, a mechanistic explanation of SEI composition and structure remains elusive. A range of theoretical techniques such as density functional theory (DFT),<sup>32,33</sup> reactive classical<sup>34,35</sup> and *ab initio*<sup>36,37</sup> molecular dynamics, and computational reaction networks (CRNs)<sup>38,39</sup> have all revealed plausible reaction pathways to key SEI components. Yet the combination of these methods has been unable to move beyond the identification of specific mechanisms towards the true formation process which involves multi-product dynamics and competitive pathways occurring on timescales ranging from picoseconds<sup>40</sup> to days.<sup>41</sup>

Here, we describe the first mechanistic, first-principles microkinetic model of SEI formation and find that it explains fundamental, observed reactive and structural trends in the LIB SEI. Using a recently developed methodology,<sup>42</sup> we analyze a CRN containing over 80 million reactions between over 5,000 species to automatically identify reaction pathways to a range of key SEI products and gaseous byproducts. Scheme 1 shows select mechanisms to form and decompose potential SEI products LEDC, LEMC, dilithium ethylene monocarbonate (DLEMC), inorganic carbonates, and  $\text{Li}_2\text{C}_2\text{O}_4$ . With rate constants derived from high-throughput transition-state calculations based on these and other predicted mechanisms (see the Supporting Information for a complete list of over 900 elementary reactions), we perform kinetic Monte Carlo (kMC) simulations to study SEI formation under varying chemical and electrochemical conditions. kMC simulations are highly attractive for modeling SEI reactivity, especially when based on high-quality thermochemical and kinetic data,<sup>43</sup> because

they can study much longer time scales than are accessible through other molecular-scale dynamical methods while retaining more mechanistic detail than mesoscale models.<sup>44,45</sup>

We perform kMC simulations under diverse chemical and electrochemical conditions in order to understand how competition between various reaction pathways could change over the course of SEI formation cycling. Most simulations begin with an initial state consisting of some amount of EC, Li<sup>+</sup>, CO<sub>2</sub>, and water. Because water will readily reduce during and even before SEI formation,<sup>46,47</sup> we include the reduction products OH<sup>-</sup> and H rather than H<sub>2</sub>O. Simulations of SEI evolution after initial formation begin with Li<sup>+</sup> and EC as well as LEDC, LEMC, Li<sub>2</sub>CO<sub>3</sub>, and Li<sub>2</sub>C<sub>2</sub>O<sub>4</sub>. To simulate SEI formation at various points during Li<sup>+</sup> intercalation (for instance in graphite<sup>48</sup> or Si<sup>49</sup> negative electrodes), we vary the electron free energy from -2.1 eV to -1.4 eV in 0.1 eV increments, corresponding to a change in the applied potential from +0.7V (roughly the reduction potential of Li<sup>+</sup>EC)<sup>50</sup> to +0.0V vs. Li/Li<sup>+</sup> (the point of lithium plating). We additionally vary the electron transport rates through application of a tunneling barrier with thickness  $D$ . Specifically, we performed simulations with  $D = 0.0\text{ \AA}$ , indicating that the electrolyte is in contact with a bare negative electrode, and with  $D = 10.0\text{ \AA}$ , indicating an existing SEI layer. Note that previous simulations have suggested that direct tunneling from the negative electrode is likely not the dominant mechanism of charge transfer during SEI growth,<sup>51,52</sup> and as a result, the variation in electron transport rate with SEI thickness  $D$  in our model is not quantitatively accurate. However, this simple method does allow for a qualitative understanding of how SEI formation varies in regimes with rapid or slow electron transport, which is a goal of this work. For each set of simulation conditions, we constructed an average kMC trajectory from 30 simulations of 10,000,000 steps each. Simulations are performed at 298.15 K (25 °C) unless otherwise noted. Further methodological details are provided in the Supporting Information.

**Recovering the Peled Model:** Figure 1 shows the average fractional quantities of gas molecules (a, b) and SEI products (c, d) as a function of applied potential and electrode



Scheme 1: Select reaction pathways involving key SEI products, including inorganic carbonates (a, b, d, e), LEDC (a, b, e), DLEM C (a, c), lithium oxalate (d), and LEMC (c). Gases  $\text{CO}_2$  (a, d, e),  $\text{C}_2\text{H}_4$  (a),  $\text{CO}$  (a, d), and  $\text{H}_2$  (c) are also highlighted. A complete set of reactions included in the microkinetic simulation are listed in the Supporting Information.

distance for a simulation beginning with 1M  $\text{Li}^+$  in a 15M EC electrolyte with  $\approx$  5ppt  $\text{CO}_2$  and  $\approx$  1ppt  $\text{H}_2\text{O}$ . Because the negative electrode can be rapidly covered by the SEI even at relatively high potentials, the electrolyte will likely not be in direct contact with the negative electrode at low potentials. Data for applied potentials below +0.5V vs.  $\text{Li}/\text{Li}^+$  with  $D = 0.0 \text{ \AA}$  are nonetheless included in Figure 1 a, c; however, the low-potential region is shaded to reflect that they may not be accessible under actual battery cycling conditions.

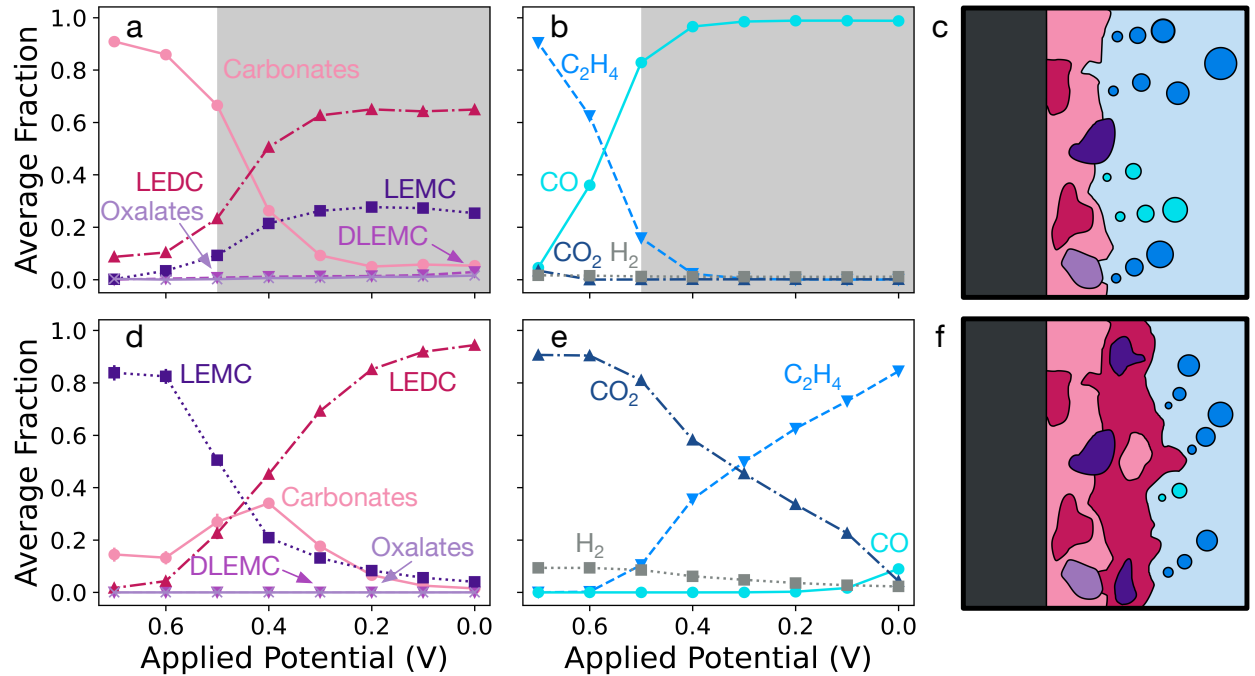


Figure 1: Average quantities of SEI products (a, d) and gaseous byproducts (b, e) at the end of kMC simulations as a function of applied potential referenced to an  $\text{Li}/\text{Li}^+$  electrode. Simulations were conducted under two conditions reflecting different regimes of SEI formation. To simulate SEI formation close to the negative electrode, before a significant interphase layer has formed (a-c), reduction was allowed to proceed in the absence of a tunneling barrier ( $D = 0.0 \text{ \AA}$ ). Because the electrode will likely be covered at high applied potentials, the low-potential region (below an applied potential of +0.5V vs  $\text{Li}/\text{Li}^+$ ) is likely not accessible in an actual battery environment. This region has therefore been shaded. To simulate SEI formation far from the negative electrode (d-f), in the presence of an existing, partially electronically insulating interphase layer, reduction was slowed by a relatively thick tunneling barrier ( $D = 10.0 \text{ \AA}$ ). Error bars representing the standard error of the mean are provided but are generally too small to be seen. Cartoons (c, f) depict the formation of SEI layers reflecting the kMC results.

The observed electrochemical competition results in a bilayer SEI structure that is in

qualitative agreement with the Peled model. When the SEI initially forms - at high potential and close to the negative electrode surface (Figure 1 a) - carbonates are the major product, with LEMC and LEDC as minority products. When reactions occur further from the negative electrode surface after this initial carbonate layer forms (Figure 1 d), LEMC and LEDC are the majority components, with inorganic carbonates as the minority components. To our knowledge, this is the first time that the varying composition of the SEI with thickness has been directly simulated from first principles. Beyond simply reproducing this structure, our microkinetic analysis is also able to suggest a mechanistic explanation for its emergence.

We observe that competition between reductive processes controls the ratio of products. When reduction rates are moderate - at high potentials close to the negative electrode (Figure 1 a-b) or at low potentials far from the negative electrode (Figure 1 d-e) - EC reduction occurs sequentially. After  $\text{Li}^+\text{EC}$  reduces once, EC ring-opens and then reduces again, ultimately producing an inorganic carbonate species (most directly  $\text{LiCO}_3^-$ ) and  $\text{C}_2\text{H}_4$  (Scheme 1 a). In the regime close to the negative electrode, the  $\text{LiCO}_3^-$  prefers to coordinate with  $\text{Li}^+$ , forming  $\text{Li}_2\text{CO}_3$ , while in the regime far from the negative electrode,  $\text{LiCO}_3^-$  often reacts with  $\text{Li}^+\text{EC}$  to form LEDC (Scheme 1 a). When reduction is more facile, a rapid two-electron reduction of EC (Scheme 1 a) can occur, resulting in CO and  $\text{Li}^+\text{OCH}_2\text{CH}_2\text{O}^{2-}$ . This pathway is dominant at moderate potentials (beginning around +0.5V vs. Li/Li<sup>+</sup>) close to the negative electrode, but it can also occur to a lesser extent at extremely low potentials (+0.0V vs. Li/Li<sup>+</sup>) far from the negative electrode. The  $\text{Li}^+\text{OCH}_2\text{CH}_2\text{O}^{2-}$  intermediate can react with one  $\text{CO}_2$  to form DLEMC, which then reacts further with  $\text{CO}_2$  to form LEDC. While  $\text{CO}_2$  may form at the positive electrode and diffuse to the negative electrode as part of a cross-talk mechanism,<sup>28</sup> for these simulations we limit  $\text{CO}_2$  to the amount that would be present in a saturated EC solution, reflecting early SEI formation conditions. Because of the limited amount of  $\text{CO}_2$ , few DLEMC or LEDC are produced by the rapid two-electron reduction mechanism. EC reduction also competes with the direct reduction of  $\text{CO}_2$  to form carbonates as well as oxalates in small quantities (Scheme 1 d).

Interestingly, we observe that the formation of LEMC is essentially unaffected by these competing reductive processes. In agreement with our recent findings based on analysis of CRNs,<sup>39</sup> the most facile path for LEMC formation is direct basic hydrolysis of  $\text{Li}^+ \text{EC}$  (Scheme 1 d). Since we assume that water reduces before significant SEI formation begins, this means that LEMC can form under any electrochemical conditions studied here. However, because we limit the initial amount of water (like  $\text{CO}_2$ ) to impurity concentrations, LEMC is a minority component except when reduction is very slow (at high potentials far from the negative electrode).

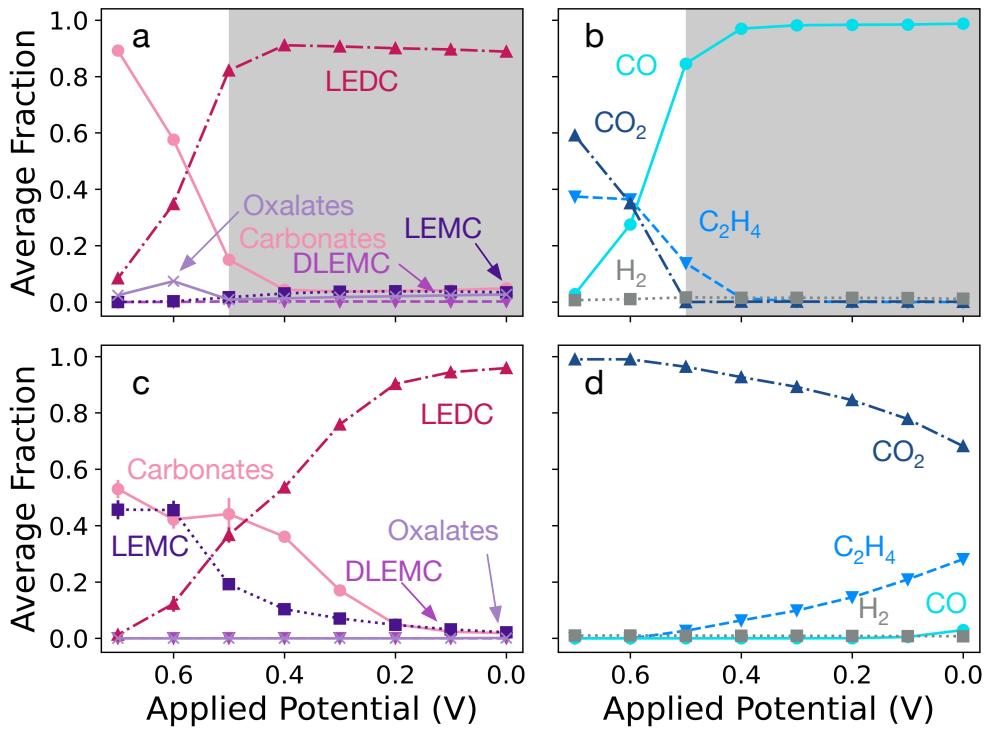


Figure 2: Average fraction of SEI products (a, c) and gaseous byproducts (b, d) at the end of kMC simulations under various applied potentials referenced to an  $\text{Li}/\text{Li}^+$  electrode with an increased initial quantity of  $\text{CO}_2$  ( $\approx 50\text{ppt}$ , 10x as much as in Figure 1). Simulations were otherwise conducted under the same conditions considered in Figure 1. Because the electrode will likely be covered at high applied potentials, the low-potential region close to the electrode (below an applied potential of  $+0.5\text{V}$  vs  $\text{Li}/\text{Li}^+$ ) is likely not accessible in an actual battery environment. This region has therefore been shaded. Error bars representing the standard error of the mean are provided but are generally too small to be seen.

**Effect of Varying Electrolyte Impurities:** In Figure 1, we find that even a small

amount of CO<sub>2</sub> is important in determining SEI composition. The critical role of impurity species in general, and CO<sub>2</sub> specifically, has long been recognized in the literature.<sup>53</sup> For EC-based electrolytes, it has been shown that the intentional addition of CO<sub>2</sub> leads to increased Li<sub>2</sub>CO<sub>3</sub> formation and improved surface passivation.<sup>23,54–57</sup> More recently, in the context of Li-ion batteries with Si negative electrodes, Schwenke et al.<sup>58</sup> found that CO<sub>2</sub> reduction prevented solvent decomposition and actually lowered the LEDC fraction in the SEI.

To further explore the effect of CO<sub>2</sub> concentration on SEI composition, we conducted additional simulations with an increased initial quantity of CO<sub>2</sub> (10x the amount in the initial simulations). Simulations with increased water content were not pursued because the initial water content of our simulations is already significantly higher than what would be expected in a rigorously dried battery electrolyte (see Supporting Information Section 1).

Figure 2 shows the average fraction of SEI products after simulations with elevated initial CO<sub>2</sub>. In agreement with the early observations of Aurbach et al.,<sup>23</sup> the quantity of inorganic carbonates produced increases significantly. With augmented CO<sub>2</sub>, carbonates are a major SEI component in the regime far from the negative electrode at moderate to high potentials (above +0.3V vs. Li/Li<sup>+</sup>). We also observe a modest increase in the formation of lithium oxalate, though it remains a minority component. In contrast with Schwenke et al., the amount of LEDC produced increases with additional CO<sub>2</sub>, especially close to the negative electrode where the additional CO<sub>2</sub> can react with the Li<sup>+</sup>OCH<sub>2</sub>CH<sub>2</sub>O<sup>2-</sup> anion along the rapid two-electron reduction mechanism of Li<sup>+</sup>EC. However, as we demonstrate below (see Exploring SEI Decomposition and Growth), LEDC that is exposed to a reducing environment should be expected to eventually decompose to form Li<sub>2</sub>CO<sub>3</sub>. Moreover, as Schwenke notes, the additional inorganic carbonate production during early SEI formation may effectively passivate the electrode surface (an effect that we have not included in our model but aim to incorporate in future work), preventing LEDC formation at lower applied potentials.

**Exploring SEI Decomposition and Growth:** The time scale accessible in a kMC simulation is limited by the fastest reactions that can occur. In our simulations - which are

able to proceed  $10^{-7}$  to  $10^{-5}$ s in 10,000,000 steps depending on simulations conditions - the fastest reactions are typically re-coordination reactions of the type  $AM+B \rightarrow A+BM$ , where  $A$  and  $B$  are coordinating molecules and  $M$  is a metal ( $\text{Li}^+$ ) (see Supporting Information). Very fast reactions also limit the sampling of rare events. In practice, these limitations prevent SEI product decomposition from being observed in our kMC trajectories. However, it is known that the SEI continues to evolve after initial formation,<sup>59</sup> and that many SEI products<sup>41</sup> are actually metastable on the time scale of battery operation. In fact, previously developed SEI formation protocols involve holding cells at elevated temperatures for hours to optimize this evolution for improved battery cell performance.<sup>60</sup>

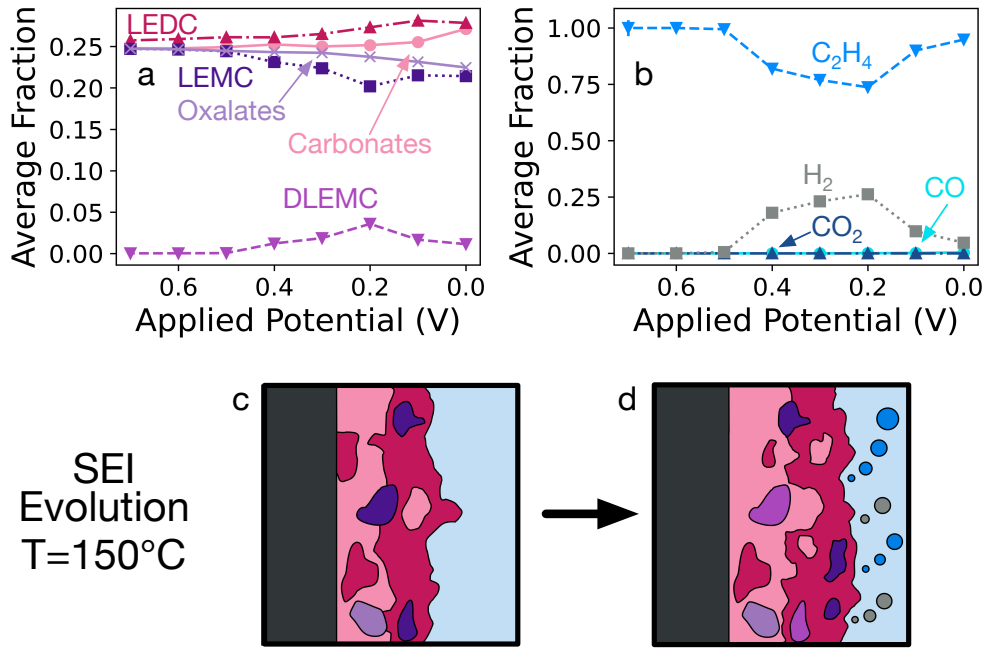


Figure 3: Average fraction of SEI products (a) and gaseous byproducts (b) at the end of kMC simulations under various applied potentials referenced to an  $\text{Li}/\text{Li}^+$  electrode with an initial state beginning with equal amounts of  $\text{LiEC}^+$ , LEDC, LEMC,  $\text{Li}_2\text{C}_2\text{O}_4$ , and  $\text{Li}_2\text{CO}_3$ . Simulations were conducted with an electron tunneling barrier of  $D = 10.0 \text{ \AA}$  to approximate the effect of a partially passivated SEI layer, which should slow reduction. To accelerate the simulation and allow for the decomposition of SEI components, an elevated temperature (423.15 K, or 150 °C) was used, and no metal re-coordination reactions were included. Error bars representing the standard error of the mean are provided but are generally too small to be seen. Cartoons (c, d) depict the evolution of an existing SEI layer, reflecting the kMC results.

In order to probe SEI evolution, we performed simulations beginning with equal amounts

of  $\text{Li}^+\text{EC}$ , LEDC, LEMC,  $\text{Li}_2\text{CO}_3$ , and  $\text{Li}_2\text{C}_2\text{O}_4$  at an elevated temperature of 423.15K (150 °C) to accelerate decomposition reactions with a tunneling barrier of  $D = 10 \text{ \AA}$ , approximating an already-formed and partially electronically insulating SEI. The rapid re-coordination reactions with  $\text{Li}^+$  were removed in order to allow us to access longer time scales of  $\approx 1\text{s}$ ; because all initial species are fully lithiated, this should not adversely affect the availability of  $\text{Li}^+$  in the simulation. In Figure 3, it can be seen that all products are relatively thermally stable at the chosen temperature (they do not react significantly at high applied potentials), though  $\text{Li}^+\text{EC}$  reduces and reacts to form some  $\text{C}_2\text{H}_4$  and additional LEDC. Under a strongly reducing potential close to the negative electrode surface, however, both LEDC and LEMC are electrochemically unstable. As has been previously observed,<sup>41</sup> LEDC decomposes to form inorganic carbonates and  $\text{C}_2\text{H}_4$  (Scheme 1 b); note that the average fraction of LEDC is not lowered because of the continual formation of LEDC by  $\text{Li}^+\text{EC}$ . Additionally, LEMC decomposes to form DLEMC and  $\text{H}_2$  (Scheme 1 d).  $\text{Li}_2\text{C}_2\text{O}_4$  and  $\text{Li}_2\text{CO}_3$  are predicted to be relatively electrochemically stable in our simulations; note that the reduced fraction of  $\text{Li}_2\text{C}_2\text{O}_4$  at low applied potentials is a result of additional LEDC forming via  $\text{Li}^+\text{EC}$  reduction, not  $\text{Li}_2\text{C}_2\text{O}_4$  decomposing.

We emphasize that while the reduction of LEMC to form DLEMC and  $\text{H}_2$  was previously postulated,<sup>27</sup> DLEMC has never before been conclusively identified by experimental spectroscopy, and this is the first direct observation of DLEMC formation by kinetic simulations. Our findings suggest that DLEMC may not be present in the SEI initially but could form over time if an SEI containing LEMC is exposed to low potentials for a prolonged period (particularly at high temperature) or cycled repeatedly. Given that previous simulations have suggested that DLEMC could be a fast  $\text{Li}^+$  conductor<sup>27</sup> and thus a beneficial SEI component, this motivates further experimental studies to confirm under what conditions DLEMC could be preferentially formed in the SEI.

**A Mechanistic Model of SEI Reactivity:** We now summarize the findings of our first-principles microkinetic modeling, using them to draw conclusions about SEI formation

and evolution. Beginning charging in the first cycle with a pristine electrode in contact with an EC electrolyte, we find that as the potential is lowered past the reduction potential of  $\text{Li}^+\text{EC}$ , EC reduces to form inorganic carbonates with some LEDC and LEMC, which we assume precipitate onto the surface. During this surface film formation,  $\text{C}_2\text{H}_4$  and CO are released. After an initial layer has formed, the potential is continually lowered over time, causing the SEI to continue to grow outward, with LEDC being the main component,  $\text{C}_2\text{H}_4$  being the major gaseous byproduct, and LEMC and inorganic carbonates being significant minority components.

After initial SEI formation is complete, the SEI can continue to evolve if exposed to low applied potentials through a potentiostatic hold or repeated cycling. Until the SEI is thick enough to be completely electronically insulating, we expect the inorganic inner region of the SEI to grow as LEDC decomposes to form inorganic carbonates and  $\text{C}_2\text{H}_4$ ; the minority LEMC will also decompose to form DLEMC and  $\text{H}_2$ . At the same time,  $\text{Li}^+\text{EC}$  reduction can continue at the electrolyte-SEI interface, leading to the formation of fresh LEDC, LEMC (if additional water is present), and inorganic carbonates.

In this work, we used kMC simulations based on reaction mechanisms obtained via automated CRN analysis and *ab initio* calculations to study SEI formation and evolution. By conducting simulations over a range of applied potentials and with varying electron tunneling barriers, we observe the formation of distinct inorganic and organic layers in the SEI, recovering and elucidating the origins of the Peled model from first principles. Competition between organic and inorganic SEI products is driven primarily by the different reduction mechanisms of  $\text{Li}^+\text{EC}$ , as well as the direct reduction of  $\text{CO}_2$ . This highlights the importance of impurity species in controlling SEI formation and supports the observation that  $\text{CO}_2$  concentration in the electrolyte can be modified to tune SEI composition. By performing simulations at elevated temperature, we observe the expected electrochemical decomposition of LEDC to form inorganic carbonates, as well as the formation of DLEMC through the reductive decomposition of LEMC. Our work demonstrates the promise of combining

first-principles and data-driven simulations with microkinetic models towards explaining the formation process of one of the most impactful passivation layers in our modern technology: the Li-ion battery SEI. In future work, we aim to expand the scope of our analysis, considering the decomposition of salts and sacrificial electrolyte additives and their effect on reactive competition in the SEI. Studies of SEI formation in next-generation battery chemistries, including multivalent-ion batteries, are also ongoing.

## Author Contributions

E.W.C.S.-S., R.L.K., D.B., and X.X. implemented kinetic Monte Carlo simulation code; T.H. determined appropriate Li re-coordination dynamics; E.W.C.S.-S. and R.L.K. generated data; E.W.C.S.-S., R.L.K., and S.M.B. analyzed data; S.M.B and K.A.P. secured funding; K.A.P. guided and supervised the work; E.W.C.S.-S. wrote the original manuscript; all authors reviewed and edited the manuscript.

## Competing Interests Statement

The authors declare no competing financial interests.

## Acknowledgement

This work was supported by the Joint Center for Energy Storage Research, an Energy Innovation Hub funded by the US Department of Energy, Office of Science, Basic Energy Sciences. Additional support comes from the Silicon Consortium Project directed by Brian Cunningham under the Assistant Secretary for Energy Efficiency and Renewable Energy, Office of Vehicle Technologies of the U.S. Department of Energy, Contract No. DE-AC02-05CH11231. D. B. and S. M. B. are supported by the Laboratory Directed Research and Development Program of Lawrence Berkeley National Laboratory under U.S. Department of Energy Con-

tract No. DE-AC02-05CH11231. Access to and assistance using the Schrödinger Suite of software tools, including Jaguar and AutoTS, was generously provided by Schrödinger, Inc. Data for this study was produced using computational resources provided by the National Energy Research Scientific Computing Center (NERSC), a U.S. Department of Energy Office of Science User Facility under Contract No. DE-AC02-05CH11231, the Eagle HPC system at the National Renewable Energy Laboratory (NREL), and the Lawrencium HPC cluster at Lawrence Berkeley National Laboratory. The authors thank Julian Self for useful discussions.

## Supporting Information Available

Computational methods; lists of molecules and reactions included in microkinetic simulations; example average trajectory; simulations with varying rates of lithium re-coordination; discussion of SEI formation with different negative electrode chemistries; discussion of the possibility of oligomerization and polymerization of byproducts of SEI formation; discussion of the rate of EC ring-opening.

## References

- (1) Yang, Y.; Xia, C.; Feng, Z.; Jiang, X.; Pan, B.; Zhang, X.; Ma, M.; Liu, R. Corrosion and passivation of annealed Ti–20Zr–6.5Al–4V alloy. *Corrosion Science* **2015**, *101*, 56–65.
- (2) Cao, F.; Song, G.-L.; Atrens, A. Corrosion and passivation of magnesium alloys. *Corrosion Science* **2016**, *111*, 835–845.
- (3) Le Guével, Y.; Grégoire, B.; Cristóbal, M. J.; Feugas, X.; Oudriss, A.; Pedraza, F. Dissolution and passivation of aluminide coatings on model and Ni-based superalloy. *Surface and Coatings Technology* **2019**, *357*, 1037–1047.

- (4) Passivation of zinc–tin–oxide thin-film transistors. *23*, L25–L27.
- (5) Zhou, L.; Bo, B.; Yan, X.; Wang, C.; Chi, Y.; Yang, X. Brief Review of Surface Passivation on III-V Semiconductor. *Crystals* **2018**, *8*, 226.
- (6) Tak, Y. J.; Keene, S. T.; Kang, B. H.; Kim, W.-G.; Kim, S. J.; Salleo, A.; Kim, H. J. Multifunctional, Room-Temperature Processable, Heterogeneous Organic Passivation Layer for Oxide Semiconductor Thin-Film Transistors. *ACS Appl. Mater. Interfaces* **2020**, *12*, 2615–2624.
- (7) Glunz, S. W.; Feldmann, F. SiO<sub>2</sub> surface passivation layers – a key technology for silicon solar cells. *Solar Energy Materials and Solar Cells* **2018**, *185*, 260–269.
- (8) Zhao, P.; Kim, B. J.; Jung, H. S. Passivation in perovskite solar cells: A review. *Materials Today Energy* **2018**, *7*, 267–286.
- (9) Winter, M. The Solid Electrolyte Interphase – The Most Important and the Least Understood Solid Electrolyte in Rechargeable Li Batteries. *Zeitschrift für Physikalische Chemie* **2009**, *223*, 1395–1406.
- (10) Xiao, C.; Usiskin, R.; Maier, J. Passivation Layers in Lithium and Sodium Batteries: Potential Profiles, Stabilities, and Voltage Drops. *Advanced Functional Materials* **2021**, *31*, 2100938.
- (11) Kern, W.; Rosler, R. S. Advances in deposition processes for passivation films. *Journal of Vacuum Science and Technology* **1977**, *14*, 1082–1099.
- (12) Metroke, T. L.; Parkhill, R. L.; Knobbe, E. T. Passivation of metal alloys using sol–gel-derived materials — a review. *Progress in Organic Coatings* **2001**, *41*, 233–238.
- (13) Hoex, B.; Schmidt, J.; Pohl, P.; van de Sanden, M. C. M.; Kessels, W. M. M. Silicon surface passivation by atomic layer deposited Al<sub>2</sub>O<sub>3</sub>. *Journal of Applied Physics* **2008**, *104*, 044903.

- (14) Xu, R.; Cheng, X.-B.; Yan, C.; Zhang, X.-Q.; Xiao, Y.; Zhao, C.-Z.; Huang, J.-Q.; Zhang, Q. Artificial Interphases for Highly Stable Lithium Metal Anode. *Matter* **2019**, *1*, 317–344.
- (15) Liu, W.; Liu, P.; Mitlin, D. Review of Emerging Concepts in SEI Analysis and Artificial SEI Membranes for Lithium, Sodium, and Potassium Metal Battery Anodes. *Advanced Energy Materials* **2020**, *10*, 2002297.
- (16) Han, J.; Nešić, S.; Yang, Y.; Brown, B. N. Spontaneous passivation observations during scale formation on mild steel in CO<sub>2</sub> brines. *Electrochimica Acta* **2011**, *56*, 5396–5404.
- (17) Bi, C.; Zheng, X.; Chen, B.; Wei, H.; Huang, J. Spontaneous Passivation of Hybrid Perovskite by Sodium Ions from Glass Substrates: Mysterious Enhancement of Device Efficiency Revealed. *ACS Energy Lett.* **2017**, *2*, 1400–1406.
- (18) Yan, S.; Song, G.-L.; Li, Z.; Wang, H.; Zheng, D.; Cao, F.; Horynova, M.; Dargusch, M. S.; Zhou, L. A state-of-the-art review on passivation and biofouling of Ti and its alloys in marine environments. *Journal of Materials Science & Technology* **2018**, *34*, 421–435.
- (19) Schneier, D.; Shaham, Y.; Ardel, G.; Burstein, L.; Kamir, Y.; Peled, E. Elucidation of the Spontaneous Passivation of Silicon Anodes in Lithium Battery Electrolytes. *J. Electrochem. Soc.* **2019**, *166*, A4020.
- (20) An, S. J.; Li, J.; Daniel, C.; Mohanty, D.; Nagpure, S.; Wood, D. L. The state of understanding of the lithium-ion-battery graphite solid electrolyte interphase (SEI) and its relationship to formation cycling. *Carbon* **2016**, *105*, 52–76.
- (21) Scully, J. R.; Inman, S. B.; Gerard, A. Y.; Taylor, C. D.; Windl, W.; Schreiber, D. K.; Lu, P.; Saal, J. E.; Frankel, G. S. Controlling the corrosion resistance of multi-principal element alloys. *Scripta Materialia* **2020**, *188*, 96–101.

- (22) Cheng, X.-B.; Zhang, R.; Zhao, C.-Z.; Wei, F.; Zhang, J.-G.; Zhang, Q. A Review of Solid Electrolyte Interphases on Lithium Metal Anode. *Advanced Science* **2016**, *3*, 1500213.
- (23) Aurbach, D.; Ein-Eli, Y.; Markovsky, B.; Zaban, A.; Luski, S.; Carmeli, Y.; Yamin, H. The Study of Electrolyte Solutions Based on Ethylene and Diethyl Carbonates for Rechargeable Li Batteries: II . Graphite Electrodes. *J. Electrochem. Soc.* **1995**, *142*, 2882.
- (24) Zhuang, G. V.; Xu, K.; Yang, H.; Jow, T. R.; Ross, P. N. Lithium Ethylene Dicarbonate Identified as the Primary Product of Chemical and Electrochemical Reduction of EC in 1.2 M LiPF<sub>6</sub>/EC:EMC Electrolyte. *J. Phys. Chem. B* **2005**, *109*, 17567–17573.
- (25) Verma, P.; Maire, P.; Novák, P. A review of the features and analyses of the solid electrolyte interphase in Li-ion batteries. *Electrochimica Acta* **2010**, *55*, 6332–6341.
- (26) Nie, M.; Abraham, D. P.; Chen, Y.; Bose, A.; Lucht, B. L. Silicon Solid Electrolyte Interphase (SEI) of Lithium Ion Battery Characterized by Microscopy and Spectroscopy. *J. Phys. Chem. C* **2013**, *117*, 13403–13412.
- (27) Wang, L.; Menakath, A.; Han, F.; Wang, Y.; Zavalij, P. Y.; Gaskell, K. J.; Borodin, O.; Iuga, D.; Brown, S. P.; Wang, C.; Xu, K.; Eichhorn, B. W. Identifying the components of the solid–electrolyte interphase in Li-ion batteries. *Nature Chemistry* **2019**, *11*, 789–796.
- (28) Rinkel, B. L. D.; Hall, D. S.; Temprano, I.; Grey, C. P. Electrolyte Oxidation Pathways in Lithium-Ion Batteries. *J. Am. Chem. Soc.* **2020**, *142*, 15058–15074.
- (29) Peled, E.; Menkin, S. Review—SEI: Past, Present and Future. *J. Electrochem. Soc.* **2017**, *164*, A1703–A1719.

- (30) Galushkin, N. ; Yazvinskaya, N. N.; Galushkin, D. N. Mechanism of Gases Generation during Lithium-Ion Batteries Cycling. *J. Electrochem. Soc.* **2019**, *166*, A897.
- (31) Rowden, B.; Garcia-Araez, N. A review of gas evolution in lithium ion batteries. *Energy Reports* **2020**, *6*, 10–18.
- (32) Wang, Y.; Nakamura, S.; Ue, M.; Balbuena, P. B. Theoretical Studies To Understand Surface Chemistry on Carbon Anodes for Lithium-Ion Batteries: Reduction Mechanisms of Ethylene Carbonate. *J. Am. Chem. Soc.* **2001**, *123*, 11708–11718.
- (33) Wang, Y.; Balbuena, P. B. Theoretical studies on cosolvation of Li ion and solvent reductive decomposition in binary mixtures of aliphatic carbonates. *International Journal of Quantum Chemistry* **2005**, *102*, 724–733.
- (34) Bedrov, D.; Smith, G. D.; van Duin, A. C. T. Reactions of Singly-Reduced Ethylene Carbonate in Lithium Battery Electrolytes: A Molecular Dynamics Simulation Study Using the ReaxFF. *J. Phys. Chem. A* **2012**, *116*, 2978–2985.
- (35) Gibson, L. D.; Pfaendtner, J. Solvent oligomerization pathways facilitated by electrolyte additives during solid-electrolyte interphase formation. *Phys. Chem. Chem. Phys.* **2020**, *22*, 21494–21503.
- (36) Leung, K.; L. Budzien, J. Ab initio molecular dynamics simulations of the initial stages of solid–electrolyte interphase formation on lithium ion battery graphitic anodes. *Physical Chemistry Chemical Physics* **2010**, *12*, 6583–6586.
- (37) Martinez de la Hoz, J. M.; Leung, K.; Balbuena, P. B. Reduction Mechanisms of Ethylene Carbonate on Si Anodes of Lithium-Ion Batteries: Effects of Degree of Lithiation and Nature of Exposed Surface. *ACS Appl. Mater. Interfaces* **2013**, *5*, 13457–13465.
- (38) Blau, S. M.; Patel, H. D.; Spotte-Smith, E. W. C.; Xie, X.; Dwaraknath, S.; Pers-

- son, K. A. A chemically consistent graph architecture for massive reaction networks applied to solid-electrolyte interphase formation. *Chem. Sci.* **2021**, *12*, 4931.
- (39) Xie, X.; Clark Spotte-Smith, E. W.; Wen, M.; Patel, H. D.; Blau, S. M.; Persson, K. A. Data-Driven Prediction of Formation Mechanisms of Lithium Ethylene Monocarbonate with an Automated Reaction Network. *J. Am. Chem. Soc.* **2021**, *143*, 13245–13258.
- (40) Leung, K. Two-electron reduction of ethylene carbonate: a quantum chemistry re-examination of mechanisms. *Chemical Physics Letters* **2013**, *568-569*.
- (41) Heiskanen, S. K.; Kim, J.; Lucht, B. L. Generation and Evolution of the Solid Electrolyte Interphase of Lithium-Ion Batteries. *Joule* **2019**, *3*, 2322–2333.
- (42) Barter, D.; Spotte-Smith, E. W. C.; Redkar, N. S.; Dwaraknath, S.; Persson, K. A.; Blau, S. M. Predictive stochastic analysis of massive filter-based electrochemical reaction networks. *ChemRxiv* **2021**, DOI:10.26434/chemrxiv-2021-c2gp3-v2.
- (43) Kuai, D.; Balbuena, P. B. Solvent Degradation and Polymerization in the Li-Metal Battery: Organic-Phase Formation in Solid-Electrolyte Interphases. *ACS Applied Materials & Interfaces* **2022**, *14*, 2817–2824.
- (44) Gavilán-Arriazu, E. M.; Mercer, M. P.; Barraco, D. E.; Hoster, H. E.; Leiva, E. P. M. Kinetic Monte Carlo simulations applied to Li-ion and post Li-ion batteries: a key link in the multi-scale chain. *Prog. Energy* **2021**, *3*, 042001.
- (45) Morgan, L. et al. Pushing the boundaries of lithium battery research with atomistic modelling on different scales. *Prog. Energy* **2021**, *4*, 012002.
- (46) Bernhard, R.; Metzger, M.; Gasteiger, H. A. Gas Evolution at Graphite Anodes Depending on Electrolyte Water Content and SEI Quality Studied by On-Line Electrochemical Mass Spectrometry. *J. Electrochem. Soc.* **2015**, *162*, A1984.

- (47) Yang, C.; Chen, J.; Qing, T.; Fan, X.; Sun, W.; von Cresce, A.; Ding, M. S.; Borodin, O.; Vatamanu, J.; Schroeder, M. A.; Eidson, N.; Wang, C.; Xu, K. 4.0 V Aqueous Li-Ion Batteries. *Joule* **2017**, *1*, 122–132.
- (48) Gallagher, K. G.; Dees, D. W.; Jansen, A. N.; Abraham, D. P.; Kang, S.-H. A Volume Averaged Approach to the Numerical Modeling of Phase-Transition Intercalation Electrodes Presented for  $\text{Li}_{\text{x}}\text{C}_6$ . *J. Electrochem. Soc.* **2012**, *159*, A2029.
- (49) Chandrasekaran, R.; Magasinski, A.; Yushin, G.; Fuller, T. F. Analysis of Lithium Insertion/Deinsertion in a Silicon Electrode Particle at Room Temperature. *J. Electrochem. Soc.* **2010**, *157*, A1139.
- (50) Xia, J.; Petibon, R.; Xiong, D.; Ma, L.; Dahn, J. R. Enabling linear alkyl carbonate electrolytes for high voltage Li-ion cells. *Journal of Power Sources* **2016**, *328*, 124–135.
- (51) Soto, F. A.; Ma, Y.; Martinez de la Hoz, J. M.; Seminario, J. M.; Balbuena, P. B. Formation and Growth Mechanisms of Solid-Electrolyte Interphase Layers in Rechargeable Batteries. *Chem. Mater.* **2015**, *27*, 7990–8000.
- (52) Single, F.; Latz, A.; Horstmann, B. Identifying the Mechanism of Continued Growth of the Solid–Electrolyte Interphase. *ChemSusChem* **2018**, *11*, 1950–1955.
- (53) Zhang, S. S. A review on electrolyte additives for lithium-ion batteries. *Journal of Power Sources* **2006**, *162*, 1379–1394.
- (54) Aurbach, D.; Chusid (Youngman), O. In situ FTIR Spectroelectrochemical Studies of Surface Films Formed on Li and Nonactive Electrodes at Low Potentials in Li Salt Solutions Containing  $\text{CO}_2$ . *J. Electrochem. Soc.* **1993**, *140*, L155–L157.
- (55) Aurbach, D.; Ein-Eli, Y.; Chusid (Youngman), O.; Carmeli, Y.; Babai, M.; Yamin, H. The Correlation Between the Surface Chemistry and the Performance of Li-Carbon

Intercalation Anodes for Rechargeable ‘Rocking-Chair’ Type Batteries. *J. Electrochem. Soc.* **1994**, *141*, 603–611.

- (56) Ein-Eli, Y.; Markovsky, B.; Aurbach, D.; Carmeli, Y.; Yamin, H.; Luski, S. The dependence of the performance of Li-C intercalation anodes for Li-ion secondary batteries on the electrolyte solution composition. *Electrochimica Acta* **1994**, *39*, 2559–2569.
- (57) Aurbach, D.; Ein-Ely, Y.; Zaban, A. The Surface Chemistry of Lithium Electrodes in Alkyl Carbonate Solutions. *J. Electrochem. Soc.* **1994**, *141*, L1.
- (58) Schwenke, K. U.; Solchenbach, S.; Demeaux, J.; Lucht, B. L.; Gasteiger, H. A. The Impact of CO<sub>2</sub> Evolved from VC and FEC during Formation of Graphite Anodes in Lithium-Ion Batteries. *J. Electrochem. Soc.* **2019**, *166*, A2035.
- (59) Barré, A.; Deguilhem, B.; Grolleau, S.; Gérard, M.; Suard, F.; Riu, D. A review on lithium-ion battery ageing mechanisms and estimations for automotive applications. *Journal of Power Sources* **2013**, *241*, 680–689.
- (60) Ellis, L. D.; Allen, J. P.; Hill, I. G.; Dahn, J. R. High-Precision Coulometry Studies of the Impact of Temperature and Time on SEI Formation in Li-Ion Cells. *J. Electrochem. Soc.* **2018**, *165*, A1529.

# For Table of Contents Only

## Mechanistic Model of the SEI

